Space-Time Structure of QCD Jets

João Silva
joao.m.da.silva@tecnico.ulisboa.pt

Instituto Superior Técnico, Lisboa, Portugal

December 2020

Abstract

Hadronic jets provide us with a rich framework for the exploration of the physics of strong interactions at multiple scales. Their evolution from an highly energetic (colored) quark or gluon to an ensemble of (color-neutral) hadrons is usually formulated in momentum space, without making reference to the space-time picture that emerges from it. However, in heavy-ion collisions, a space-time reference frame is introduced by the interaction of jets with the *Quark-Gluon Plasma*, the hot and dense medium existing in the first instants of our Universe's lifetime. Motivated by that, this work is an investigation of the space-time structure of QCD jets that propagate in vacuum.

By approximating a jet's development by a clustering history, the timescales (*formation times*) involved are calculated and an absolute time order of the splittings is presented. Formation times are shown to span multiple orders of magnitude. It is verified not only that they are exactly ordered along the branches of a history assigned by the τ reclustering algorithm, but also that they are logarithmically separated. Furthermore, one makes explicit that different reclustering algorithms result in different space-time structures for the same jet. The first splitting's timescale, however, is shown to be independent of the choice of algorithm. Additionally, one presents a simple strategy to estimate this particular formation time through experimentally measurable quantities.

Keywords: Quantum Chromodynamics; Jet; Branching history; Formation time; Space-time structure.

1 Introduction

1.1 Motivation and Overview

Over the past few decades, we have witnessed numerous ultra-relativistic hadronic collision experiments with increasing energy, whether it be between proton beams (pp) or heavy nuclei beams. These experiments, carried out most recently by the Large Hadron Collider (LHC) and the Relativistic Heavy-Ion Collider (RHIC), allow us to study, among a wide range of aspects of particle physics, the theory of the strong interaction, namely Quantum Chromodynamics (QCD).

The analytical equations governing the evolution of QCD systems and usual parton shower Monte Carlos are formulated in momentum space. This is usually studied without ever detailing what the actual space-time evolution is. Where and when does the first particle emission happen after a quark or a gluon has been produced in the hard scattering of a collision event? Is this question relevant for a QCD jet propagating freely in vacuum? No. Is it relevant for a QCD jet produced in heavy-ion collisions? Absolutely. In such events, a background medium is produced - the *Quark-Gluon Plasma* (QGP) - which introduces a space-time reference frame in which jets propagate. Let us introduce this complex QCD state of matter for the purpose of motivating the study of the space-time structure of QCD jets.

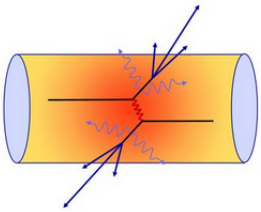

Figure 1: Pictoric overview of an example of an heavy-ion collision's components (QGP + back-to-back jets) [1].

In a typical heavy-ion collision, two nuclei collide at ultra-relativistic energies and, aside from the hard perturbative scatterings which give rise to hadronic jets, the majority of these interactions will involve little transverse momentum transfer. These are called "soft" processes and they are the main reason why both the energy and particle densities rise abruptly shortly after (~ 1 fm/c) the collision [2] - the QGP is created (Fig. 1). This deconfined,

hot and dense state of matter, with energy densities of about 20 times those inside typical hadrons [2], has been thoroughly investigated in distinct experiments and it is supported by unequivocal evidence (see, e.g., [3]). Being the state of matter that permeated our Universe in its first few μs of existence, it is only natural that one is interested in studying it.

The QGP holds its distinct properties until the local energy density falls below that of a typical hadron, which happens on a timescale of ~ 10 fm/c. Jets, which have to plough through the medium, will then suffer a wide range of modifications by scattering off its constituents - *jet quenching* [4]. The degree to which a jet is modified is a great footprint of what happened inside the QGP's during its lifetime. In practice, by comparing jets with and without the presence of the medium (e.g. pp collisions), one can infer information about its properties.

If, in particular, one wishes to access the spatio-temporal evolution of the QGP, then one needs to be sensitive to its characteristic timescales. Modified in-medium jets may provide insights on the relevant space-time regions for jet-plasma interactions. To leverage this information and extract knowledge about the QGP's spatial and temporal profiles, it is imperative that one attributes a space-time meaning to each of the jet's emissions.

The probing of the temporal evolution of the QGP has already been approached in a number of works. For instance, motivated by experimental evidence of unchanged fragmentation patterns of in-medium jets, Casalderrey-Solana *et al* [5] concluded that roughly 70% of the relevant branching process will always occur outside the medium. In a more recent work, Apolinário *et al* [6] worked on using the top quark to extract meaningful information about the QGP's time structure. Lastly, recent efforts were carried out by [7], where the authors introduce the τ algorithm and conclude, using the first emission's formation time as a metric, that it maximizes the correlation between the reclustered branching history and the corresponding Monte Carlo parton shower information.

1.2 Objectives

The main aim of this thesis is to explore the timescales involved in the transition from a single hard parton to a multi-parton ensemble. The framework for this study is the production of QCD jets - multi-particle final states which are footprints of this quantum evolution - in high-energy proton-proton (pp) collisions, i.e., *vacuum* jets. One formulates this evolution in a simplistic manner and solely by resorting to final state information, i.e., the jet's constituents. First, one assigns a *branching history* to each jet and then quantifies the relevant timescales through the calculation of *formation times* of intermediate virtual states. The result is a space and time meaning to the parton shower interpretation of multiple parton emissions. The space-time structure that is obtained from this process is often put into perspective by having the lifetime of the *Quark-Gluon Plasma* as a reference timescale.

2 Theoretical Background

In this section, one will introduce key concepts which form the basis for the remaining of the work, detailing the two centerpiece concepts - assignment of a *branching history* and the *parton formation time*.

2.1 QCD Basics

Quantum Chromodynamics (QCD) is the theory that describes the strong interaction between the constituents of the subatomic particles called hadrons, e.g., protons and neutrons, the components of atomic nuclei. These constituents, quarks and gluons, are defined by their transformation properties under representations of SU(3), i.e., the theory is non-Abelian, which, by introduction of the *color* quantum number, implies that the gluon self-interacts. Among other repercurssions, this causes QCD to possesse the feature of *asymptotic freedom* - strength of the interaction decreases with increasing momentum and with corresponding decreasing distance. This in opposition to QED, where the charge *screening* effect dominates. This *anti-screening* effect is made explicit by QCD's running of the coupling:

$$\alpha_s(Q^2) = \frac{\alpha_s(\mu^2)}{1 + b_0 \alpha_s(\mu^2) \ln(Q^2/\mu^2)} \tag{1}$$

with $b_0 = \frac{11N_c - 2n_f}{12\pi}$ and μ the renormalization scale. Often, one writes Eq. (1) in terms of a mass scale which is generated as a consequence of renormalization - the QCD scale $\Lambda_{QCD} \approx 200$ MeV, sufficiently above which, i.e., in high energy processes, one can use perturbative QCD (pQCD). Another consequence of Eq. (1) is that, at large distances, QCD is strongly interacting, with quarks and gluons bounded within hadrons, leading to *color confinement* - only color-singlet particles, i.e., hadrons, are detected.

2.2 Jets and Parton Showers

Jets are produced in collision events and are detected as relatively isolated bunches of energy in the form of collimated sprays of hadrons. They can be thought of as footprints of the theory's colored degrees of freedom produced in rare short-distance (hard) interactions, carrying information about physics at multiple scales.

The process of their evolution, whereby one goes

from a single parton being produced off the hard collision at large angles to a multitude of hadrons being detected, can be phrased as a conjugation of higher order (perturbative) corrections to the hard process - the emission of an arbitrary number of partons - and of an *hadronization* (non-perturbative) phase - the conversion of the final partons into hadrons. The multiple emission of partons is usually seen at the light of the *parton-shower* representation - a probabilistic interpretation of a jet's evolution as a sequence of $1 \to 2$ factorized collinear emissions and which one simulates via Monte Carlo methods by choosing an appropriate *ordering variable*.

The starting point for the simulation of a parton shower is the single emission probability. This probability, in the collinear limit, for massless partons and to first order in α_s is given by:

$$d\mathcal{S}_{i\leftarrow j} = \frac{\alpha_s}{2\pi}\hat{P}^{(0)}_{i\leftarrow j}(z)dz\frac{dQ^2}{Q^2}\frac{d\phi}{2\pi} \tag{2}$$

where the functions $\hat{P}^{(0)}_{i\leftarrow j}(z)$ are the unregularized, leading-order (LO) splitting functions. This expression turns explicit the non-integrable *double-log divergences* common to most pQCD calculations. One has a *soft* divergence $z \to 0$ contained in the splitting function and a *collinear* divergence present in dQ^2/Q^2.

A single collinear emission is usually generalized to multiple collinear emissions by the *Sudakov* form factor, where one rather approaches the problem through the *no-emission* probability. The Sudakov represents the no-emission probability off parton species j between Q^2 and Q_0^2:

$$\Delta_i(Q^2, Q_0^2) = \exp\left[-\sum_j \int_{Q_0^2}^{Q^2} \frac{dQ'^2}{Q'^2}\int dz \frac{\alpha_s(Q'^2)}{2\pi}\hat{P}^{(0)}_{j\leftarrow i}(z)\right] \tag{3}$$

where the azimuthal angle ϕ was integrated out. The Sudakov factor, in conjugation with the DGLAP (Dokshitzer–Gribov–Lipatov–Altarelli–Parisi) equations, the QCD evolution equations, provides a picture of multiple collinear emissions as an evolution process, whether it is the evolution of an initially colliding parton - *Initial State Radiation* (ISR) - or the evolution of a hard-scattered parton - *Final State Radiation* (FSR).

2.3 Jet Reconstruction and Branching Histories

Jet finding in an event is performed via *jet algorithm* - a set of rules to cluster the particles' four-momenta into jets. In addition to the algorithm and its parameters, like the *jet radius* $R \sim 1$, one needs to specify a recombination scheme, which dictates how to add the 4-momentum of the two combined particles. Together, these two form a *jet definition*, i.e., a connection between what can be calculated and what is measured. In this work, we focus on sequential recombination algorithms with the *E-scheme*. These algorithms look pairwise at the 4-momenta of all particles in an event and combine them according to a certain distance metric. In particular, we will use the *generalized-k_t algorithms* [8], whose distance metric is:

$$d_{ij} = \min(p_{t,i}^{2p}, p_{t,j}^{2p})\Delta R_{ij}^2, \qquad d_{iB} = p_{t,i}^{2p}R^2 \tag{4}$$

The *anti-k_t algorithm* [9] ($p = -1$), which is currently the standard algorithm used at the LHC experiments for jet finding, is the one used for that purpose in this work. The main reason for this is that it is practically insensitive to extra soft radiation.

Interestingly enough, this algorithmic process may be taken outside the context of jet finding and be used to assign a clustering sequence to a jet, which can be a representation of a jet's internal evolution - its *fragmentation history*. This task boils down to building a hierarchy of $1 \to 2$ emissions - from a set of final-state particles which belong to a reconstructed jet, sequentially *cluster* them until there is only one resultant particle. This is often called a *reclustering procedure*, where each merging step is seen as a *splitting*, and each cluster's 4-momentum is identified with a virtual particle.

For this purpose, one will use generalized-k_t algorithms for $p = 0,\ 1/2,\ 1$ and, also, the *Jade algorithm* [10]. Their respective distance metrics are small whenever the QCD branching process is kinematically enhanced. For $p = 1$, one obtains the *k_t-algorithm* [11], which is particularly useful for dividing jets into a number of hard subjets. For $p = 0$, one obtains the *C/A algorithm* [12], which resolves a jet based on its angular structure, resulting in a tree structure which mimics an *angular-ordered* shower. Finally, for $p = 1/2$, one has the *τ algorithm* (see, e.g., [7]) whose distance metric, as we shall in Section 4.4, is proportional to the inverse of an approximation of the parton formation time introduced in Section 2.4. As such, a resulting branching tree which is ordered in formation time.

The four reclustering algorithms are said to be LL equivalent. Although a brief comparison between them is drawn in Section 4.3, one will focus mainly on the τ algorithm for the remaining of the analysis.

2.4 From Parton Formation Time to Jet Space-Time Structure

It can be said that a virtual parton, i.e. an off mass-shell parton emerging from some process, lives for a certain amount of time before it radiates another parton. One can think of this quantity as how long

it takes for a parton to become an independent colored object, i.e., a source of further colored particles [13]. Throughout this work, one shall refer to this lifetime as the *formation time* of the subsequent pair of states a virtual state evolves into. A naive estimate of it can be made by resorting to the Heisenberg's uncertainty principle [13] $t_{rest}m \sim 1$ and Lorentz boosting the result to the laboratory frame:

$$\tau \sim \frac{E}{m^2} \equiv \tau_0 \tag{5}$$

where one is working in natural units, i.e, $\hbar = c = 1$. One shall refer to this formation time as the *exact estimate* for the remaining of this work.

With a branching history assigned to a jet and a formation time associated with each of the splittings in it, one can further calculate a *space-time* structure. In this work, two ways of *ordering splitting* are taken into account - the reclustering order (inverse sequence by which partons were recombined) and the increasing *absolute time* order, which imposes an absolute time scale (denoted by $\Sigma\tau$ in Section 4.5.1) to the fragmentation history. It does so by recursively summing formation times along the tree - $(\Sigma\tau)^i = \sum_j^i \tau^j$, where the j index is a symbol for every parton that comes before parton i in the branch it belongs to.

3 Simulation and Reconstruction Setup

In this work, we chose to study QCD *vacuum* jets in pp collisions, generating events with Pythia 8.2.35 [14] (Tune 4C). We simulate 10^6 events at a CM energy of 5 TeV. The sequential recombination algorithms Section 2.3 used in both clustering and reclustering procedures, along with any extracted jet kinematical information, are dealt with by resorting to Fastjet 3.3.2 [8]. We'll be focusing on events of the type Z+jet (Fig. 2). The process is generated with pure Z contributons, i.e., there is no interference term between photon and Z production. Furthermore, the Z boson's decay is turned off. In terms of kinematic cuts, the products of the hard scattering are forced to have a transverse momenta above 90 GeV and the events are only accepted for Z bosons with transverse momenta $p_t^Z \geq 100$ GeV and rapidities $|y^Z| \leq 2$. Furthermore, one reweights events through `PhaseSpace:bias2SelectionPow = 6.3`. For jet reconstruction, one uses the anti-k_t algorithm and the jet radius $R \sim 1$. With regard to kinematical acceptance criteria, the final partons are filtered according to $p_t^{\text{parton}} \geq 0.5$ GeV and $|y^{\text{parton}}| \leq 3.5$ and we'll be working with jets with transverse momenta $p_t^{\text{jet}} \geq 20$ GeV and rapidities $|y^{\text{jet}}| \leq 2.5$. The reconstructed jet and the Z boson should be separated azimuthally by $\Delta\phi = 7\pi/8$. The jet reclustering radius is necessarily larger than the clustering one.

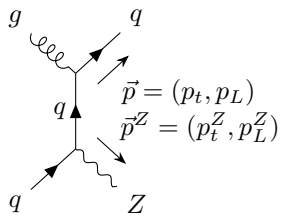

Figure 2: Example of an hard interaction diagrams for a Z+jet event type, along with kinematics of the hard scattered particles. Because we assume the initial partonic collision carries no transverse momentum, we necessarily have $p_t = p_t^Z$. Hence, in this work, an idealized jet reconstruction would have $p_t^{jet}/p_t^Z = 1$.

4 Results Analysis

An exposition of this work's main results is made in the following sections.

4.1 Reconstruction efficiency and ISR

In our work, the aim is to capture most FSR, i.e., an optimal reconstruction of the hard scattered parton's 4-momentum (Fig. 2). A smaller radius may reconstruct a "fat" jet as two smaller jets and a larger radius would cause more ISR to contaminate our ideally reconstructed jet. Hence, there is a need for a trade-off between capturing FSR and supressing the impact of ISR.

One can quantify the efficiency, i.e., how much of the FSR we include, by evaluating the ratio the jet and the Z's p_t. In Fig. 3a and 3b, one shows how this ratio changes when we open up our jet's radius. Although not represented here, jet radii $R < 1$ do not perform optimally in reconstruction - they miss out on a significant portion of the FSR shower's content - and $R = 1.75$ is, as expected, the one which better reconstructs FSR. In spite of this, adding ISR causes a significant increase of the distribution's tail for ratios above 1 when going from $R = 1$ (Fig. 3a) to $R = 1.75$ (Fig. 3b). This suggests that using the larger radius ($R = 1.75$) causes ISR to take over the jet's radiation content. Hence, reconstruction radii in the range $R \in (1, 1.75)$ seem to be the best compromise.

4.2 First splitting's formation time

The parton formation time derived in Section 2.4 (Eq. (5)) only depends on the 4-momentum of the parton we are considering. This implies, in particular, that the parton leading to the first splitting (the "seed" parton), has an algorithm independent formation time. It depends, however on what one captures inside the jet.

Because we are using the E-scheme, the seed parton's 4-momentum is exactly equal to the reconstructed jet's, making the first splitting's formation time uniquely dependent on the experimentally

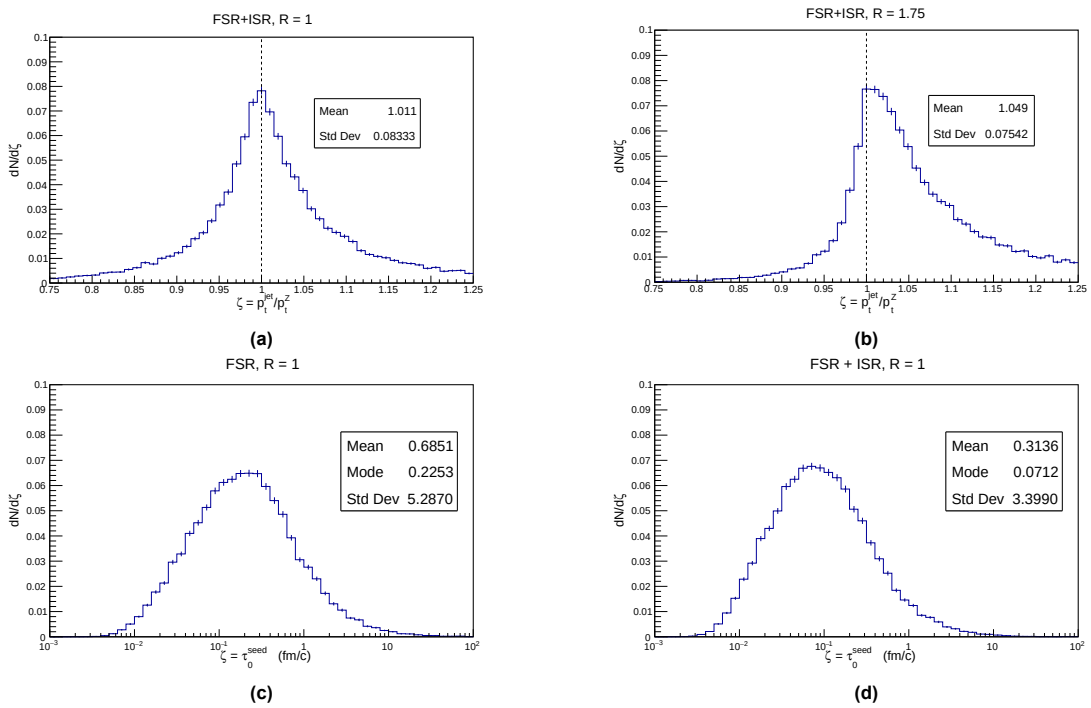

Figure 3: Ratios p_t^{jet}/p_t^Z for two jet radii a) $R = 1$ and b) $R = 1.75$, with Initial State Radiation. First splitting's formation time distributions for events of c) FSR and d) FSR+ISR, with jet radius $R = 1$. All distributions are normalized to unit integrals.

measurable jet kinematic variables:

$$\tau_0^{\text{seed}} = \frac{E^{\text{jet}}}{(m^{\text{jet}})^2} = \frac{p_t^{\text{jet}}\sqrt{1+(m^{\text{jet}}/p_t^{\text{jet}})^2}\cosh y^{\text{jet}}}{(m^{\text{jet}})^2} \tag{6}$$

The relevance of this conclusion is that this quantity, as one shall see in Section 4.5.1, is a proxy for the shortest timescale inside a jet whose branching history is calculated with the τ algorithm [7].

4.2.1 Sensitivity to ISR

In Fig. 3d one presents the distribution of the first splitting formation time (Fig. 3c) when adding ISR. This causes an overall downshift of the distribution and a decrease in the mean value. If we consider that this radiation is mainly soft then, considering Eq. (6), an increase in jet mass is responsible for such effect. Althought not shown here, a similar effect seems to happens when adding hadronization, with the difference that the bulk of the distribution is squeezed into a smaller range of values. Overall, both modules seem to cause a suppression of larger formation times. For the remaining sections of this work one will focus on jets reconstructed with radius $R = 1$.

4.2.2 Correlation with Jet Mass

An interesting follow-up question is whether one can reduce the kinematic dependences in Eq. (6) to a single experimentally measurable quantity, taking the remaining dependences into account through a dispersion measure. Judging by Eq. (6), the jet mass m^{jet} seems a reasonable choice, with dispersion taken into account by the energy spectrum. Looking at Fig. 4a, where the mean values follow an almost straight line, one concludes that, approximately for all jets masses, one has $\sigma_\tau/\langle\tau\rangle \sim 0.5$. A more accurate prediction of the seed formation time demands a cut in the jet's phase space. In Fig. 4b, one plots the same quantities of Fig. 4a, but for 4 distinct $p_t \cosh y$ bins with the same 100 GeV width. For the $p_t \cosh y$ bin that results in the largest dispersion (the red markers), one can expect the seed formation time to be within a relative interval of no more than $\sim 20\%$ around the mean value.

4.3 Reclustering algorithm comparison

In Fig. 5, one compares the ratios of average formation times of each splitting between jet histories calculated with the 4 different algorithms (Section 2.3), having the τ algorithm as reference. Looking at both plots one concludes that, with or without ISR and hadronization, the τ space-time structure attributes, on average, larger formation times than the remaining algorthims. One can further conclude that the most striking differences are seen in earlier splittings and this is amplified when one includes ISR and works at hadron-level (Fig. 5b). Nonetheless, the mean formation times of each branching tree are of the same order for every splitting and differ, at most, by $\sim 25\%$.

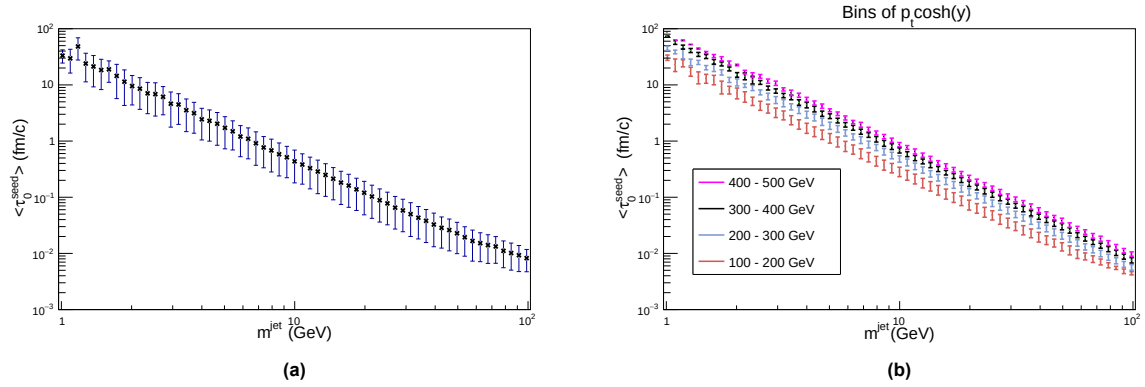

Figure 4: a) Average first splitting formation time for each jet mass in the range 1 GeV $< m^{\text{jet}} < 200$ GeV, along with the standard deviation calculated for each mass bin. b) Same result for various $p_t \cosh y$ bins. All results are parton-level.

4.4 Formation Time Estimates and Kinematical Dependences

Let us focus on parton-level FSR showers and branching histories calculated with the τ algorithm from now on.

4.4.1 Local Approach

Consider the calculation of the parton formation time introduced in Eq. (5) by taking into account the kinematics of the two subsequent partons. The virtuality m^2 of the parent parton can be written as:

$$m^2 = \sum_i m_i^2 + 2p_{t,1}p_{t,2}(\sqrt{1+m_1^2/p_{t,1}^2}\times \sqrt{1+m_2^2/p_{t,2}^2}\cosh(\Delta y_{12}) - \cos(\Delta\phi_{12})) \tag{7}$$

where $\Delta y_{12} = y_1 - y_2$, $\Delta\phi_{12} = \phi_1 - \phi_2$ and one used the 4-momentum in terms of collider variables $p^\mu = (m_t\cosh y, p_t\cos\phi, p_t\sin\phi, m_t\sinh y)$. From Eq. (7), one concludes that even if a particle splits into two almost collinear particles, its formation time is not necessarily large because the subsequent particles may have a non-negligible virtualities.

Expressing the energy of the initial parton as $E = E_1 + E_2$, the formation time in Eq. (5) can be written in terms of collider variables and the children partons virtualities. One can then work with various kinematic limits (Eq. (8). By ignoring the parton virtualities m_i^2 in the denominator one obtains τ_1 and, by neglecting the remaining virtuality terms $m_i^2/p_{t,i}^2$, one obtains τ_2. Then, τ_3 and τ_4 are the collinear and soft limits, applied on τ_2. The estimate τ_4 is exactly the inverse of the distance metric of the τ clustering algorithm (Section 2.3) multiplied by $\cosh y$, motivating Section 4.5.1.

A comparison between τ_i (cumulative) and $\overline{\tau}_i$ (isolated) is shown in Fig. 7a and 7b, where the ratios with respect to the exact estimate τ_0 were calculated. The central conclusions concern virtualities. When we look at the ratio of τ_1 in Fig. 7b, we confirm that ignoring the m_i^2's altogether is the the most impactful approximation. Then, in comparing Fig. 7a and 7b, it is made clear that the approximations are not independent of each other. For instance, one has that $\tau_2 \sim 2\overline{\tau}_2$.

4.4.2 Global Approach

Now consider the parton formation time calculation solely from final-state partons. Because we are working with the E-scheme, every parton's 4-momentum is simply the sum of the 4-momenta of a subset of all the final partons. Hence, the virtuality of the parton is:

$$m^2 = \left(\sum_i p_i\right)^2 = \sum_i\sum_j p_{t,i}p_{t,j}(\sqrt{1+m_i^2/p_{t,i}^2}\times \sqrt{1+m_j^2/p_{t,j}^2}\cosh(\Delta y_{ij}) - \cos(\Delta\phi_{ij})) \tag{10}$$

where $\Delta y_{ij} = y_i - y_j$, $\Delta\phi_{ij} = \phi_i - \phi_j$ and the i and j indices run over a subset of all the final partons - those belonging to branches which go through the parton we are considering. To calculate the formation time one would divide the sum of the relevant energies $E = \sum_i E_i$ by Eq. (10). Consequently, the formation time of a given parton does not depend on its subsequent branching history but simply on what final partons emerge from it, confirming that the first splitting's formation time is independent of the reclustering algorithm. One can now work with the similar kinematic limits of Eq. (8), but now we are not restricted to pairs of clustered partons (Eq. 9). All approximations are analogs of the local approach applied to final partons, with the soft limit (τ_4^g) being framed as a final parton which is much more energetic than all the other partons in the relevant subset, h being its index in Eq. (9).

In Fig. (7c and 7d), one shows a comparison between τ_i^g (cumulative) and $\overline{\tau}_i^g$ (isolated). First of all, ignoring all terms containing masses is still not a

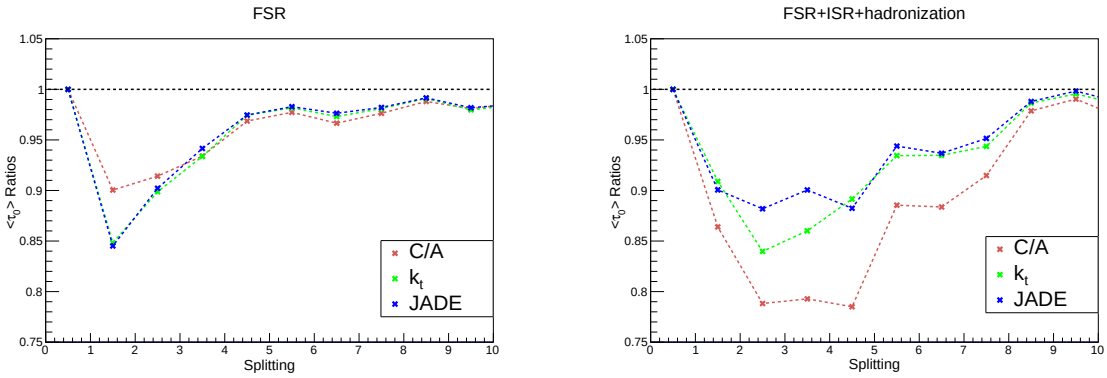

Figure 5: Ratios of the mean formation times of each splitting, ordering them according to their absolute time and having the τ algorithm as a reference. Results are presented for the remaining algorithms, for the first 10 splittings and for events of a) FSR and b) FSR+ISR+hadronization.

reasonable approximation (τ_2^g in Fig. 7c). Solely ignoring $m_i^2/p_{t,i}^2$ implies only minor deviations ($\overline{\tau}_2^g$ in Fig. 7d), smaller than what we observed for the local approach in ($\overline{\tau}_2$ in Fig. 7b). Neglecting m_i^2 with respect to every $p_j \cdot p_k$ (τ_1^g) is the most impactful approximation.

4.5 Space-Time Structure Analysis

The assignment of a space-time structure to a jet prompts basic questions such as "what are the orders of magnitude of the timescales involved in a jet's development?" and "are the splittings of each branch well separated in time?".

4.5.1 Formation Time Orderings

In Section 2.3, one mentioned that τ a branching history would be ordered in formation times. The motivation for this assertion is the expression for τ_4 in Eq. (8) - $\tau_4 = \cosh y / d_{ij}^{\tau}$. In fact, one verified this to be true for the majority of cases, with only very few where the ordering is spoiled by the term $\cosh y$ - only about 0.02% of the splittings. Interestingly enough, one also found that, for $\tau_0 = E/m^2$, this ordering is exact (Fig. 8a). Additionally, as can be seen in Fig. 8a, the formation times are logarithmically separated inside each branch, with an average factor of order 10 between them.

Despite this exact ordering along branches, τ_0 is not necessarily ordered along the reclustering sequence - most likely a consequence of branch alternation in the sequence. This is in agreement with usual parton shower generators where, although each branching is ordered according to a given quantity, distinct branches have their own logarithmic separation between consecutive splittings.

A question one could then ask is if the splitting order resulting from calculating absolute times is exactly the same as the one resulting from the reclustering procedure. In Fig. 8b, the distribution of the ratios $(\Sigma\tau_0)^i/(\Sigma\tau_0)^{i-1}$ for consecutive reclustering steps is presented. It is clear that the answer is negative - there are plenty of cases, about 17%, where the ordering is not verified. Nevertheless, this is still true on average.

4.5.2 Formation Time Distribution

The distribution of formation times along the splittings of a jet (Fig. 8c) allows one to have different "representations" of the same jet at different frames of its temporal development - particularly

$$
\begin{aligned}
\tau_1 &\equiv \frac{E}{m^2 - \sum_i m_i^2} \\
\tau_2 &\equiv \frac{p_{t,1}\cosh y_1 + p_{t,2}\cosh y_2}{2p_{t,1}p_{t,2}\left(\cosh(y_1 - y_2) - \cos(\phi_1 - \phi_2)\right)} \\
\tau_3 &\equiv \frac{(p_{t,1} + p_{t,2})\cosh y}{p_{t,1}p_{t,2}\Delta R^2} \\
\tau_4 &\equiv \frac{\cosh y}{\min(p_{t,1}, p_{t,2})\Delta R^2}
\end{aligned}
\tag{8}
$$

$$
\begin{aligned}
\tau_1^g &\equiv= \frac{E}{m^2 - \sum_i m_i^2} \\
\tau_2^g &\equiv \frac{\sum_i p_{t,i}\cosh y_i}{\sum_i \sum_{j\neq i} p_{t,i}p_{t,j}\left(\cosh(\Delta y_{ij}) - \cos(\Delta\phi_{ij})\right)} \\
\tau_3^g &\equiv \frac{2\sum_i p_{t,i}\cosh y^{jet}}{\sum_i \sum_{j\neq i} p_{t,i}p_{t,j}\Delta R_{ij}^2} \\
\tau_4^g &\equiv \frac{2p_{t,h}\cosh y^{jet}}{\sum_i \sum_{j\neq i} p_{t,i}p_{t,j}\Delta R_{ij}^2}
\end{aligned}
\tag{9}
$$

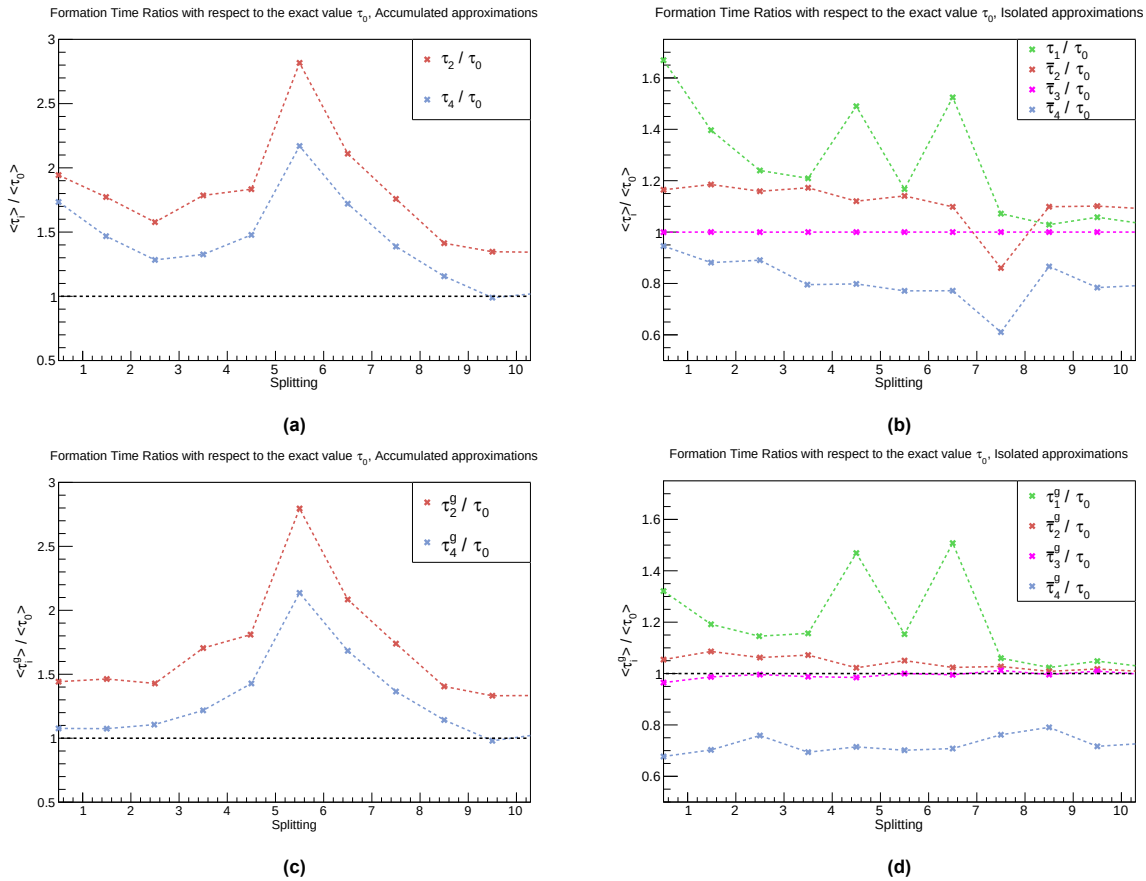

Figure 7: Ratio of the average formation times, with respect to the exact estimate τ_0, for a) τ_2 and τ_4, defined in Eq. (8), b) $\overline{\tau}_i$, c) τ_2^g and τ_4^g, as defined in Eq. (9) and d) $\overline{\tau}_i^g$. All results are parton-level and the formation times $\overline{\tau}_i$ and $\overline{\tau}_i^g$ are defined as those which contain a single approximation, with i corresponding to the numbers in Eqs. (8) and (9). For instance, $\overline{\tau}_2$ results from only neglecting terms $m_i^2/p_{t,i}^2$ while keeping the remaining terms intact, like the m_i^2 in the denominator and $\overline{\tau}_4^g$ results from simply taking the energy as that of the hardest final parton.

useful when studying the QGP. However, we face ourselves with a startling result: formation times inside a jet span approximately 12 orders of magnitude in fm/c. Nonetheless, at least for the first ~ 20 splittings, peak formation times are well defined and most of the distribution is contained in a smaller span of orders of magnitude. What remains of the dispersion in the distribution's bulk is probably caused by the inclusive nature of the plot.

The span of multiple orders of magnitude is not, however, so puzzling if we examine the dependences on $\tau_0 = E/m^2$ for internal partons of the branching history - the transverse momentum ($p_t \approx E/\cosh y$) covers about 3 orders of magnitudes and the virtualities range from about $\sim 10^2$ GeV to almost real partons ($m \approx 0$ GeV). These partons with negligible virtuality result from recombining a pair of massless and almost collinear final partons, thus resulting in disparately large formation times - see Eq. (7). This is supported by the right hand side plot in Fig. 8d, where one can clearly sees that formation times above 10^4 are only found for partons separated by $\Delta R < 10^{-2}$, which represents about 0.01% of the distribution. This implies that most very large formation times are not even detected in usual calorimeters, which have a finite angular resolution. Not only this, but, for QGP studies, any intra-jet activity occurring after 10 fm/c does not influence the plasma-jet interaction. Note that this cut is also neglecting splittings with $\tau_0 < 10$ fm/c, as can be seen in Fig. 8d. However, such splitting's subsequent partons, being collinear, would presumably not be resolved as separate color charges by the medium (see, e.g., minimum resolution length in ([15]).

Moreover, fixing the number of jet splittings (Fig. 9, 10 splittings), reveals that the later splittings are the ones causing most of the dispersion. In spite of the clear decrease in dispersion, there is still a span of about 3 or 4 orders of magnitude which, presumably, is a consequence of the probabilistic nature of parton shower generation. Hence, calculations which depend on parton formation times will always have this associated dispersion. This is specially relevant in splittings whose distributions have relevant tails at values of order 10 fm/c, if one

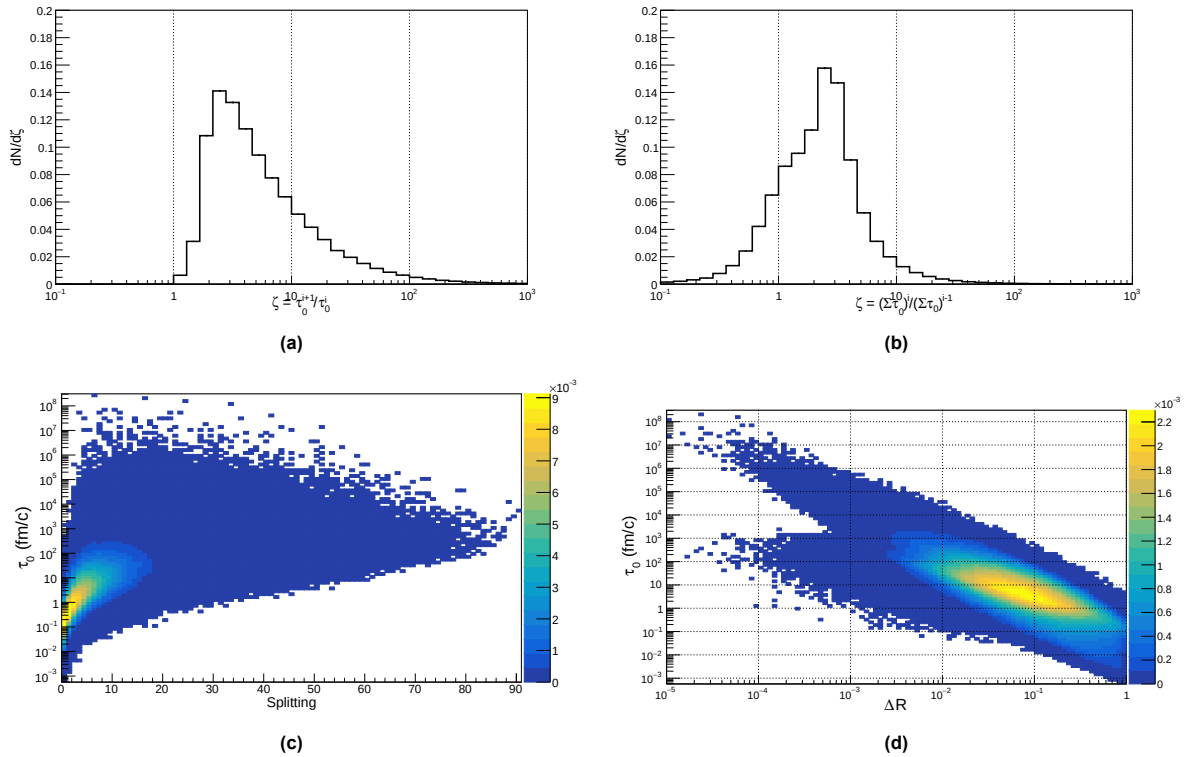

Figure 8: Ratio of a) the formation times τ_0 of partons i and $i+1$ in each branch, b) absolute times $\Sigma\tau_0$ of consecutive reclustering steps i and $i-1$. The plots are normalized to unit integrals and resulted from data of all generated events. c) Scattering plot for the formation time of each splitting according to their order in absolute time. d) Scattering plot of the formation time of each splitting and corresponding ΔR of the subsequent partons.

is working with jet-quenching models with a dependence on parton formation time (e.g. [5]). A very important observation to make from the plots in Fig. 10 is how the whole line of average formation times decreases when one increases the jet particle multiplicity. This suggests that one should select jets with higher multiplicities in order to be more sensitive to the medium's initial instants.

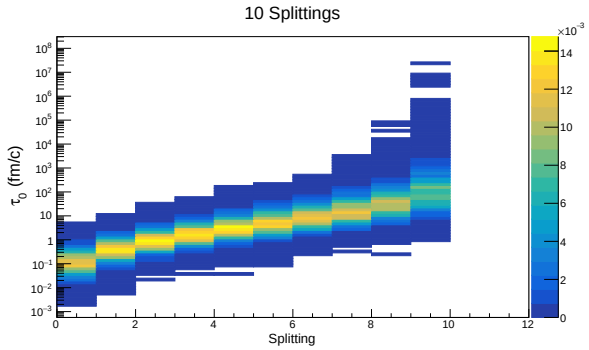

Figure 9: Scattering plot for the formation time of each splitting according to their absolute time, for a jet with 10 splittings. The result is parton-level.

5 Main Achievements

In this work, we set out to understand the relevant timescales involved in the space-time evolution of a jet. The obtained results can be reproduced by generating events in the working conditions described in Section 3.

First, one understood that there must be a compromise between efficiently capturing most of the FSR and avoiding to reconstruct ISR in a jet. Consequently, the jet reconstruction radius should not be increased recklessly. This is particularly important because the formation times are sensitive to the presence of this additional, mostly soft radiation. The usage of grooming techniques would be relevant in the future.

Following this, we concluded that the seed formation time is the shortest timescale for a jet with a τ branching history and that it is independent of the algorithm chosen for reclustering. It is dependent on the efficiency which one captures FSR. We saw, with parton-level FSR, that by selecting a narrower region of the jet's $p_t \cosh y$ while making a single experimental measurement - the jet's mass - one can determine the first splitting's formation time with a relative dispersion of, at most, 20% in our working conditions. Future relevant work may include studying how first splitting's formation time relates to the findings in [7].

We then verified that different reclustering algorithms generate different space-time structures for

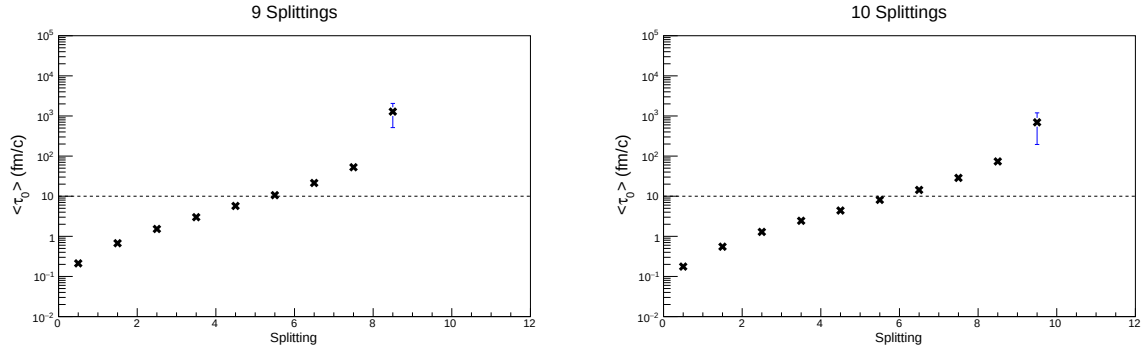

Figure 10: a),b) Average of formation time for each splitting, with errors given by the standard error of the mean (SEM). The jet multiplicity is fixed in each plot at a) 9 and b) 10 splittings. All results are parton-level.

the same jet. The dissimilarities are most significant in early splittings, where the jet's activity matters the most with respect to the QGP. It would be relevant to explore the phase space differences between algorithms so as to make the space-time structure algorithm-invariant.

As for the formation time's kinematic dependences, it was made clear, for the local approach, that ignoring m_i^2 results in an overestimation which can go up to orders of magnitude in a few specific cases. In the global approach, one turned explicit that a branching tree's formation time can be calculated solely through final-state information. Additionally, one concluded that it only matters what final partons belong to the subjet emerging from an "internal" parton.

Following this, one verified that not only are formation times ($\tau_0 = E/m^2$) exactly ordered along the branches of the jet's tree, but the consecutive formation times are logarithmically separated. Additionally, one concluded that, much like in parton shower generation, different branches have different logarithmic orderings. Finally, we understood that, because of the large available phase space for the substructure constituents, formation times inside a jet span about 12 orders of magnitude. This dispersion is mostly caused by large formation times coming from the last splittings in a jet, which, for the most part, are not detected. Furthermore, the bulk (90%) of the distribution lies in, approximately, 5 orders of magnitude, a reflection of the inclusive nature of the results. Fixing the jet's multiplicity revealed a very well defined trend of the mean formation times. Most importantly, one found, that jets with higher multiplicity tend to have a greater sensitivity to the medium's initial timescales.

Acknowledgements

The author would like to thank Prof. G. Milhano and Prof. L. Apolinário for their patience and fruitful discussions. The financial support by Fundação para a Ciência e a Tecnologia (Portugal) under project CERN/FIS- PAR/0024/2019 is acknowledged.

References

[1] M. van Leeuwen. Results of the ALICE experiment. *54 Int. Winter Meet. on Nuc. Phys.*, 2016.

[2] Busza, Wit and Rajagopal, Krishna and van der Schee, Wilke. Heavy Ion Collisions: The Big Picture and the Big Questions. *Annual Review of Nuclear and Particle Science*, 68(1):339–376, 2018.

[3] (J. Adams et al.), STAR Collaboration. *Nucl. Phys.*, A757:102, 2005.

[4] Mehtar-Tani, Yacine and Milhano, J. Guilherme and Tywoniuk, Konrad. Jet Physics in Heavy-Ion Collisions. *International J. of Modern Physics A*, 28(11):1340013, 2013.

[5] Casalderrey-Solana, Jorge and Milhano, José Guilherme and Quiroga-Arias, Paloma. Out of medium fragmentation from long-lived jet showers. *Physics Letters B*, 710(1):175–181, Mar 2012.

[6] Liliana Apolinário and José Guilherme Milhano and G. P. Salam and Carlos Salgado. Probing the Time Structure of the Quark-Gluon Plasma with Top Quarks. *Physical review letters*, 120 23: 232301 , 2018.

[7] Liliana Apolinário and André Cordeiro and Korinna Zapp. Time reclustering for jet quenching studies, 2020.

[8] Matteo Cacciari, Gavin P. Salam, and Gregory Soyez. FastJet User Manual. *Eur. Phys. J. C*, 72:1896, 2012.

[9] Cacciari, Matteo and Salam, Gavin P and Soyez, Gregory. The anti-ktjet clustering algorithm. *Journal of High Energy Physics*, 2008(04):063–063, Apr 2008.

[10] W. Bartel et al. Experimental Studies on MultiJet Production in e^+e^- Annihilation at PETRA Energies.

[11] S. Catani, Yu.L. Dokshitzer, M.H. Seymour, and B.R. Webber. Longitudinally-invariant $k_\perp$-clustering algorithms for hadron-hadron collisions. *Nuclear Physics B*, 406(1):187 – 224, 1993.

[12] Dokshitzer, Yu.L and Leder, G.D and Moretti, S and Webber, B.R. Better jet clustering algorithms. *Journal of High Energy Physics*, 1997(08):001–001, Aug 1997.

[13] Yuri L. Dokshitzer, A. Khoze, Alfred H. Mueller, and S.I. Troian. *Basics of perturbative QCD*. 1991.

[14] Sjöstrand, Torbjörn et al. An introduction to PYTHIA 8.2. *Computer Physics Communications*, 191:159–177, Jun 2015.

[15] Jorge Casalderrey-Solana, Yacine Mehtar-Tani, Carlos A. Salgado, and Konrad Tywoniuk. New picture of jet quenching dictated by color coherence. *Physics Letters B*, 725(4):357 – 360, 2013.